

Article

Enhanced Degradation of Decabromodiphenyl Ether via Synergetic Assisted Mechanochemical Process with Lithium Cobalt Oxide and Iron

Xiaoyi Lou ¹, Yifan Sui ², Qichao Zhang ², Changling Fang ¹, Yunyu Tang ¹, Xuan Zhang ¹, Guangxin Yang ¹, Yongfu Shi ¹, Dongmei Huang ^{1,*} , Jie Guan ² and Yaoguang Guo ^{2,*} 

- ¹ Laboratory of Quality Safety and Processing for Aquatic Product, East China Sea Fisheries Research Institute, Chinese Academy of Fishery Sciences, Shanghai 200090, China; huoxingmayi@126.com (X.L.); fangling0334081@163.com (C.F.); hi_tyy@163.com (Y.T.); zhangxuan0430@163.com (X.Z.); guo5142@126.com (G.Y.); xyzmn530@sina.com (Y.S.)
- ² Shanghai Collaborative Innovation Centre for WEEE Recycling, School of Resources and Environmental Engineering, Shanghai Polytechnic University, Shanghai 201209, China; sui yifan333@163.com (Y.S.); cscr007@163.com (Q.Z.); guanjie@sspu.edu.cn (J.G.)
- * Correspondence: hdm2001@126.com (D.H.); yguo@sspu.edu.cn (Y.G.)

Abstract: The removal of decabromodiphenyl ether (BDE 209), as a typical persistent organic pollutant (POP), is of worldwide concern. Mechanochemical (MC) processes are promising methods to degrade environmental pollutants, most of which use a single grinding reagent. The performance of MC processes with co-milling agents still needs to be further verified. In this study, an efficient MC treatment with combined utilization of lithium cobalt oxide (LiCoO₂) and iron (Fe) as co-milling reagents for BDE 209 degradation was investigated. The synchronous action of LiCoO₂ and Fe with a LiCoO₂/Fe/Br molar ratio of 1.5:1.67:1 and a ball-to-powder ratio of 100:1 led to almost thorough-paced abatement and debromination of BDE 209 within 180 min using a ball milling rotation speed of 600 rpm. The reduction in particle sizes and the destruction of crystal structure in mixture powders with the increase in milling time induced the enhanced degradation of BDE 209, as characterized by scanning electron microscopy (SEM) and X-ray diffraction (XRD). The X-ray photoelectron spectroscopy (XPS) characterization showed that the valence state of Co was converted from Co(III) to Co(II), and Fe(0) was changed to Fe(III) when treated with an MC process. This indicated that the reductive debromination of BDE 209 by Fe and the following oxidative degradation of debrominated products by LiCoO₂ were integrated in a concerted way. It proved the removal of BDE 209 via an MC treatment. The full breakage of C-Br and C-O bonds in BDE 209 was confirmed by Fourier transform-infrared spectrometry (FT-IR) spectra, and a possible abatement pathway was also proposed based on the identified intermediate products using gas chromatography–mass spectrometry (GC-MS). These obtained results indicated that a combination of LiCoO₂ and Fe as co-milling reagents is promising in the MC treatment of toxic halogenated pollutants like BDE 209.

Keywords: decabromodiphenyl ether; iron; lithium cobalt oxide; mechanochemical process; synergetic effect



Citation: Lou, X.; Sui, Y.; Zhang, Q.; Fang, C.; Tang, Y.; Zhang, X.; Yang, G.; Shi, Y.; Huang, D.; Guan, J.; et al. Enhanced Degradation of Decabromodiphenyl Ether via Synergetic Assisted Mechanochemical Process with Lithium Cobalt Oxide and Iron. *Appl. Sci.* **2023**, *13*, 12924. <https://doi.org/10.3390/app132312924>

Academic Editor: Gerald Sims

Received: 20 October 2023

Revised: 16 November 2023

Accepted: 21 November 2023

Published: 2 December 2023



Copyright: © 2023 by the authors. Licensee MDPI, Basel, Switzerland. This article is an open access article distributed under the terms and conditions of the Creative Commons Attribution (CC BY) license (<https://creativecommons.org/licenses/by/4.0/>).

1. Introduction

Polybrominated diphenyl ethers (PBDEs) have been widely used as brominated flame retardants in manufactured products, such as plastics, construction materials, textiles, and electronic equipment [1–4]. Decabromodiphenyl ether (BDE 209) is one of the commercial PBDEs found worldwide [5,6]. However, BDE 209 is one of the typical persistent organic pollutants (POPs), with characteristics of long transportation range and environment persistence, due to its indestructible chemical bonds making it difficult to be decomposed [7,8]. Previous studies have consistently found BDE 209 in different parts of the environment,

such as air, water, soil, and sediment [9–13]. Moreover, due to its high lipophilicity, BDE 209 can be accumulated in biological organisms and eventually transferred to humans through the food chain. It has been reported that BDE 209 exposure might lead to neurotoxicity, endocrine disruption, and carcinogenicity [14,15]. Thus, the elimination of BDE 209 has been currently capturing increased attention worldwide.

Recently, many studies have focused on the degradation of BDE 209 via chemical oxidation techniques, such as incineration, Fenton reaction, or photocatalytic oxidation [16–18]. Each of these methods, however, has its limitations. Incineration generates secondary hazardous byproducts, such as polychlorinated dibenzo-*p*-dioxins, leading to secondary pollution [18]. As for advanced oxidation processes, namely the Fenton reaction and photocatalytic oxidation, they have been employed to decompose BDE 209 in liquid media [19]. However, its high hydrophobicity gives BDE 209 the tendency to enrich in solid matrices, which may significantly decrease the efficiency of the degradation treatment. Thus, it is urgent to develop new technologies to degrade BDE 209 in the solid phase. Recently, mechanochemical (MC) techniques based on grinding reactants in the solid phase have attracted particular attention as straightforward procedures for treating halogenated organic pollutions. In the MC procedure, solid-to-solid reactions are triggered by collisions with milling bodies in reaction devices [20]. Compared to the chemical oxidation approaches, the MC method holds an advantage due to its use of mild temperature and pressure, the absence of organic solvent, and the avoidance of emission of hazardous byproducts [21].

It has been proven that the grinding reactant is one of the key elements in the MC process, having significant impacts on the degradation efficiency of halogenated organics. In general, the common co-milling reagents employed for organic decomposition can be divided into two main groups, reductive agents such as zero-valent metals (e.g., Fe, Al) [22,23] and oxidative substances like persulfate and manganese dioxide [24,25]. During the MC processes, zero-valent irons (ZVIs) are utilized as electron donors to accomplish the reductive dehalogenation of the target chemicals [26]. For oxidative degradation of halogenated pollution, the MC process is mainly activated by losing electrons to oxidants. Manganese dioxide is usually used as the electron acceptor of the redox couples $\text{Mn(IV)} \rightarrow \text{Mn(II)}$ or $\text{Mn(IV)} \rightarrow \text{Mn(III)}$ [27]. The above-mentioned MC methods are all conducted using a single milling reagent. Recently, the combination of reductive metals and oxides has been tested to improve the destruction efficiency of halogenated contaminants in MC treatment [28–30]. Zhang et al. researched the synergistic action of Bi_2O_3 and Fe on the MC process for BDE 209 degradation [31]. The results showed that the destruction efficiency using Fe and Bi_2O_3 is significantly higher than those using only Fe or Bi_2O_3 under comparable operational conditions.

Lithium cobalt oxides (LiCoO_2), the cathode material of lithium-ion batteries (LIBs), have a certain oxidation capacity, as cobalt can be reduced from Co(III) to Co(II). Saeki et al. proposed an MC method for extracting the valuable metals Li and Co from LiCoO_2 with polyvinyl chloride (PVC) as a co-grinding reagent [32]. It is interesting to note that inorganic chlorides were detected in the MC products as about 90% of the chlorine in PVC had been transformed. This might suggest that LiCoO_2 could be applied to degrade halogenated organics in MC treatment. ZVI, as a cheaper but strong electron donor, has an excellent reductive dehalogenation efficiency in both liquid solvents and MC processes. In our previous study [33], reductive iron (Fe) powder could significantly promote the extraction efficiency of Li and Co from waste lithium cobalt oxide batteries via the MC process, and the valence state of Co was converted from Co(III) to Co(II) after an MC reductive process with Fe. Therefore, we anticipated that the combination of LiCoO_2 and Fe could improve the destruction of halogenated organics via the MC process.

Hence, the objective of the present study was to investigate the degradation behavior of BDE 209 with the assistance of LiCoO_2 and Fe by implementing the MC method. The MC parameters including the molar ratio of LiCoO_2/Fe , rotational speed, and ball-to-powder ratio were examined. The physical chemistry changes were characterized by scanning electron microscopy (SEM), X-ray diffraction (XRD) meter, X-ray photoelectron

spectroscopy (XPS), and Fourier transform-infrared spectrometry (FT-IR). Ultimately, the intermediate products of BDE 209 were detected by GC-MS to illustrate the details of the mechanism of the BDE 209 degradation. As such, it will offer new insights with regard to both the resource utilization of the cathode material LiCoO_2 from the increasing number of spent LIBs and the elimination of POPs.

2. Experimental

2.1. Materials and Reagents

Decabromodiphenyl ether (BED 209, 99%) was obtained from Alfa Aesar. Lithium cobalt oxide (LiCoO_2 , 99.8%) was purchased from Aladdin Co., Ltd., Shanghai, China. Reductive iron powder (Fe, >98%) was supplied by Sinopharm Chemical Reagent Co., Ltd., Beijing, China. Acetonitrile and tetrahydrofuran (THF) of chromatographic grade were from Shanghai Macklin Biochemical Technology Co., Ltd., Shanghai, China. All the other chemical reagents were analytical grade and used without further purification. Milli-Q ultrapure water ($18.2 \text{ M}\Omega\cdot\text{cm}$) was used for all the experiments.

2.2. MC Treatments

MC experiments were carried out using a planetary ball mill (QM-QX04, Nanjing University Instrument Corporation, Nanjing, China) at 25°C and standard atmosphere conditions. In each trial, 0.46 g of BDE 209 powder was blended with LiCoO_2 and Fe in a mortar in specific ratios. The mixture was then transferred into stainless-steel pots, and steel balls with a diameter of 6 and 10 mm were added. To determine the optimal experimental conditions, the ratio of $n_{\text{LiCoO}_2}:n_{\text{Fe}}$ was varied from 0.36 to 1.08, as the amount of LiCoO_2 increased gradually, and the $n_{\text{Fe}}:n_{\text{Br}}$ was fixed at 1.67:1, maintaining the amount of BDE 209 at 0.48 mM. The balls-to-powder mass ratio ranged from 50:1 to 200:1. The rotational speed was adjusted from 300 to 700 rpm, with automatic rotation direction changes every 15 min. Control experiments involved milling BDE 209 with Fe only, LiCoO_2 only, or without additives. Most batch experiments were duplicated, with an error of less than 3%.

2.3. Analysis

To determinate the degradation of BDE 209, 0.1 g of milled mixture was collected and subjected to extraction with THF (50 mL) through ultrasonic treatment for 20 min. After centrifugation at 1.0×10^4 rpm for 5 min, the supernatant was filtered with a $0.22 \mu\text{m}$ membrane. The extracted liquid underwent analysis for BDE 209 concentration using high-performance liquid chromatography (HPLC, LC-20A, Shimadzu, Kyoto, Japan) equipped with an SPD-20A UV detector at 230 nm with an Athena C18 column ($4.6 \text{ mm} \times 250 \text{ mm}$, $5 \mu\text{m}$). The mobile phase consisted of 95% acetonitrile and 5% water, with a flow rate of 1.0 mL/min.

The extracted solution underwent additional analysis employing a gas chromatograph-mass spectrometer (GC-MS, Agilent 7890B-5977B, Santa Clara, CA, USA) to identify the intermediate products of BDE 209. A DB-5HT ($30 \text{ m} \times 0.25 \text{ mm} \times 0.25 \mu\text{m}$) capillary column was employed with helium gas serving as the carrier at a flow rate of 1 mL/min. Injection of $1 \mu\text{L}$ of the sample occurred in splitless mode, while the injector temperature was maintained at 250°C . The temperature program followed the following steps: 100°C held for 2 min, increased to 200°C at $40^\circ\text{C}/\text{min}$, elevated to 330°C at $20^\circ\text{C}/\text{min}$, then held at 330°C for 2 min. The ion source temperature was set at 230°C , with an electron energy of 70 eV and a scan mass (m/z) range from 20 to 800. Analysis of the products was referenced against the NIST 08 mass spectrometry library.

An additional 0.1 g of milled mixture was extracted by 50 mL ultrapure water under ultrasonic concussion for 20 min, followed by centrifugation. The supernatant was then filtered with $0.22 \mu\text{m}$ membrane. This solution was utilized for monitoring bromide ion concentration with a Dionex ICS-2100 ion chromatography equipped, with a Dionex IonPac

AS18-4 μM anion exchange column (4×150 mm). The debromination efficiency of BDE 209 could be evaluated by Equation (1) [34]:

$$\text{Debromination} = \frac{C_t}{C_0} \times 100\% \quad (1)$$

where C_t is the content of inorganic Br^- at ball milling time t ; C_0 is the initial content of total bromine in BDE 209.

FT-IR measurement (VERTEX 70, Bruker, Saarbrücken, Germany) was implemented to detect the chemical structure changes of BDE 209 during the MC process based on the standard KBr method. The microscopic appearance was recorded using SEM (JSM 6400, JEOL, Tokyo, Japan). The element valence was characterized by XPS (Kratos AXIS Ultra DLD, Shimadzu, Kyoto, Japan) with a monochromatic Al K_α X-ray source. XRD analysis (D8 Advance, Bruker, Saarbrücken, Germany) was conducted to determine the phases and crystal structure of the milling mixtures using Cu K_α radiation at a scan speed of 8° (2θ) per minute ranging from $2\theta = 10^\circ$ to 70° . The full width at half maximum (FWHM) of peaks, crystal size, and degree of disorder were calculated using Jade 6.0, and the degree of disorder in the MC process was obtained from Equation (2) [35]:

$$\eta = \left(1 - \frac{\sum I_{\text{Activated}}}{\sum I_{\text{Raw}}}\right) \times 100\% \quad (2)$$

where η is the degree of disorder (%), $\sum I_{\text{Raw}}$ is intensity of each crystal plane diffraction peak for raw samples, and $\sum I_{\text{Activated}}$ is the intensity of each activated crystal plane diffraction peak for activated samples.

3. Results and Discussion

3.1. Performance of BDE 209 Degradation

To investigate the impact of co-milling agents, BDE 209 was decomposed via the MC process employing LiCoO_2 Fe powder separately, a mixture of LiCoO_2 and Fe, and a control without additives (Figure 1). The results revealed that the degradation rate of BDE 209 was only 13.5% within 300 min without a grinding reagent. When LiCoO_2 or Fe was added individually, there was a modest increase, with removal rates of 34.6% and 59.3% for BDE 209 within 300 min, respectively. However, the simultaneous addition of Fe and LiCoO_2 significantly enhanced the decomposition of BDE 209, achieving a remarkable removal rate of 99.8% after 180 min. This indicates a synergistic effect in the degradation of BDE209 in the MC treatment when Fe and LiCoO_2 are used in combination. Therefore, subsequent experiments were performed to explore the influence of milling conditions on the decomposition and debromination of BDE 209, with both Fe and LiCoO_2 participating in the MC process within a milling time of 240 min.

3.2. Effect of Milling Conditions on BDE 209 Degradation and Debromination

The impact of milling conditions is illustrated in Figure 2 through quantification of the decomposition and debromination efficiency of BDE 209. Further details are provided in the Supplementary Materials (Figures S1–S3). As seen in Figure 2a, the effect of the grinding reagent molar ratio between LiCoO_2 and Fe ($n_{\text{LiCoO}_2}/n_{\text{Fe}}$) was investigated, and BDE 209 exhibited a faster degradation with a higher $n_{\text{LiCoO}_2}/n_{\text{Fe}}$ ratio after 240 min co-milling. When $n_{\text{LiCoO}_2}/n_{\text{Fe}}$ increased from 0.36 to 0.9, the reduction of BDE 209 was rapidly and significantly escalated from 23.5% to 99.9%, while the debromination rate was varied from 21.0% to 92.0%. However, with $n_{\text{LiCoO}_2}/n_{\text{Fe}}$ reaching 1.08, the removal of BDE 209 remained almost constant, while the debromination decreased to 79.0%. In the low $n_{\text{LiCoO}_2}/n_{\text{Fe}}$ range, the higher LiCoO_2 load enhanced the oxidation of BDE 209. Conversely, in the high $n_{\text{LiCoO}_2}/n_{\text{Fe}}$ range, the excessive LiCoO_2 oxidized the Br^- yielded in the MC process to Br_2 , leading to a low Br^- concentration being detected, and consequently the debromination rate being decreased [36].

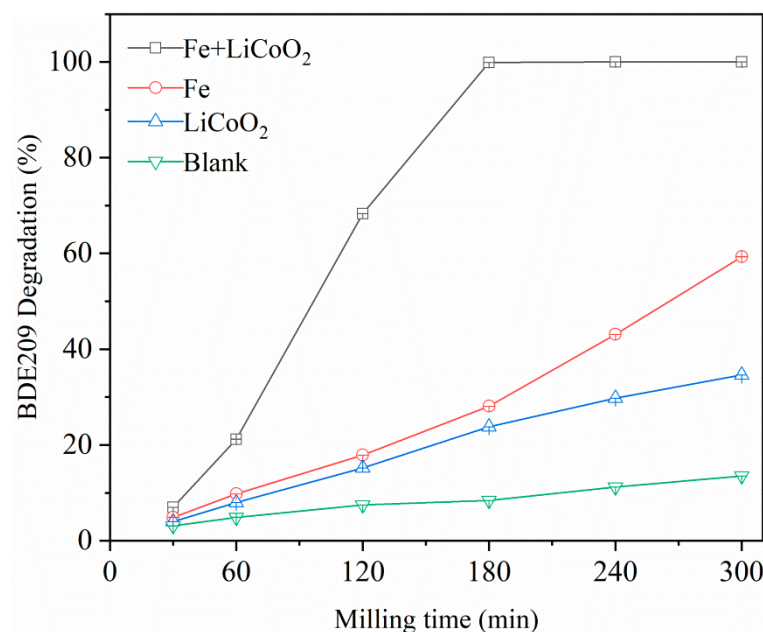


Figure 1. MC degradation of BDE 209 with different co-milling reagents. Conditions: $m_{\text{BDE 209}} = 0.46$ g, $n_{\text{LiCoO}_2}/n_{\text{Fe}}/n_{\text{Br}} = 1.5:1.67:1$, rotation speed = 600 rpm, ball-to-powder mass ratio (m_b/m_p) of 100:1.

Figure 2b presents the influence of the rotational speed on the abatement and debromination of BDE 209 within 240 min. As the rotational speed varied from 300 to 600 rpm, both the removal and debromination of BDE 209 increased, reaching a maximum of 99.9% and 92.0% at 600 rpm, correspondingly. These results suggest that a higher ball milling speed could lead to a better degradation and debromination of BDE 209. Previous studies confirmed that the impact energy is a key factor in the MC treatment of pollutants, (see Equation (3)) [37,38]. The faster rotation speed increases the collision velocity and collision number per unit time, leading to a higher impact energy of the MC process [38]. Hence, the C-C and C-Br bonds in BDE 209 are broken more easily with higher impact energy. When the rotation speed increased to 700 rpm, the degradation and debromination rates remained stable. This indicates that an excessively high rotation speed is unnecessary in this combined system, thus saving energy consumption:

$$E = \sum_{j=1}^n \frac{m_b}{2m_p} v_j^2 \quad (3)$$

where E is the impact energy of milling balls, v_j is the relative speed of the impact between the ball and the tank wall or the balls, m_b is the mass of milling balls, n is the collision number per unit time, and m_p is the mass of sample powders charged into the mill pots.

Figure 2c depicts the effect of the ball-to-powder ratio (m_b/m_p) on the removal and the debromination of BDE 209 during MC treatment. The results indicate a positive correlation between the degradation rate and the yield of Br^- with m_b/m_p . As m_b/m_p was set at 50, the removal of BDE 209 was 52.1%, and the debromination was 48.9%; as m_b/m_p increased to 100, 150, and 200, the removal rate reached nearly 100%, and the debromination was 93.1% when m_b/m_p was at 200. The swift removal of BDE 209 was attributed to the large number of balls at high m_b/m_p , increasing the collision frequency per unit time, and consequently, the amount of impact energy transferred to the solid particles becoming higher (Equation (3)) [39]. It is important to note that the higher the m_b/m_p ratio, the higher is the energy consumption [37–39]. Hence, the m_b/m_p value of 100 was selected as the optimal experimental parameter, considering operability and cost of practical application.

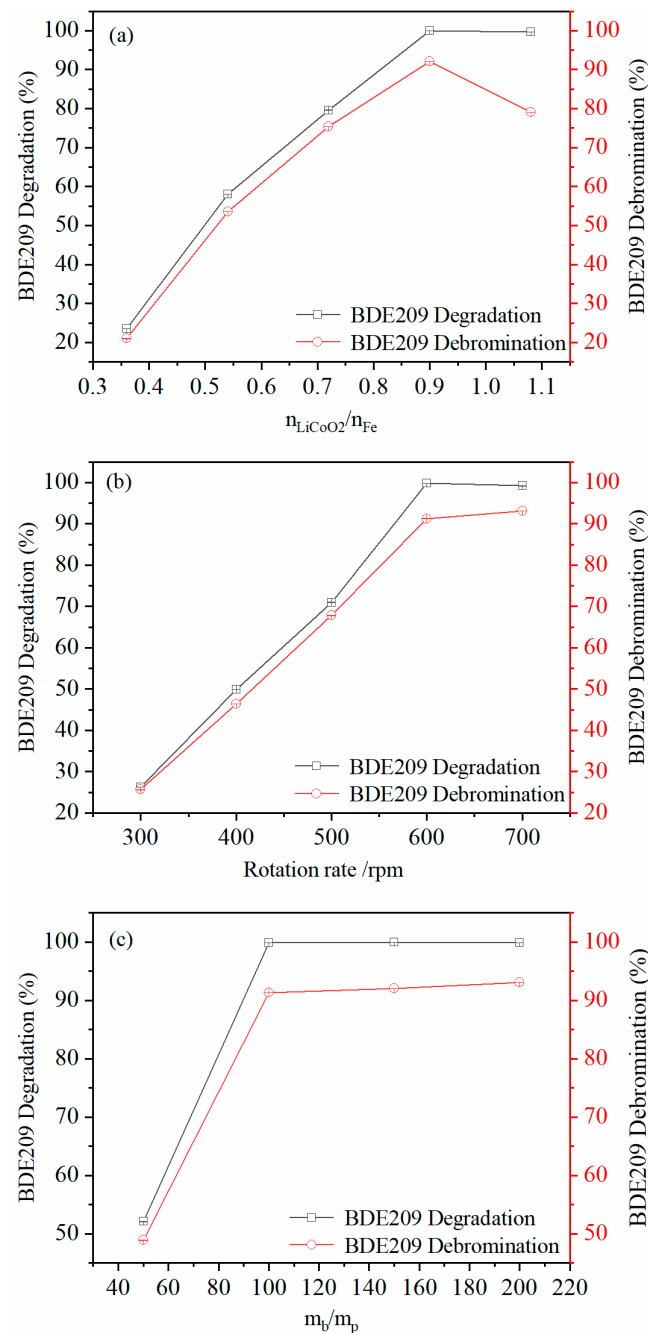


Figure 2. Degradation and debromination of BDE 209 at different ball milling conditions in 240 min. Conditions: (a) The effect of grinding reagent molar ratio between LiCoO_2 and Fe ($n_{\text{LiCoO}_2}/n_{\text{Fe}}$) with rotation speed of 600 rpm, and ball-to-powder mass ratio (m_b/m_p) of 100:1. (b) The effect of rotation rate with $n_{\text{LiCoO}_2}/n_{\text{Fe}}/n_{\text{Br}} = 1.5:1.67:1$, and m_b/m_p of 100:1. (c) The effect of ball-to-powder mass ratio with $n_{\text{LiCoO}_2}/n_{\text{Fe}}/n_{\text{Br}} = 1.5:1.67:1$, and rotation speed of 600 rpm.

3.3. Characterization Analysis and Mechanism

3.3.1. SEM Analysis

To elucidate the detailed reaction mechanism, physical chemical property changes of the sample powders were examined. Figure 3 shows the morphology of activated samples at different ball-milling times as observed by SEM. It can be seen that the surfaces of the particles became significantly rougher with the extended milling time. These outcomes imply that substantial energy was generated during the MC process and transferred to

the samples, resulting in the samples being damaged and inducing the degradation and debromination of BDE 209.

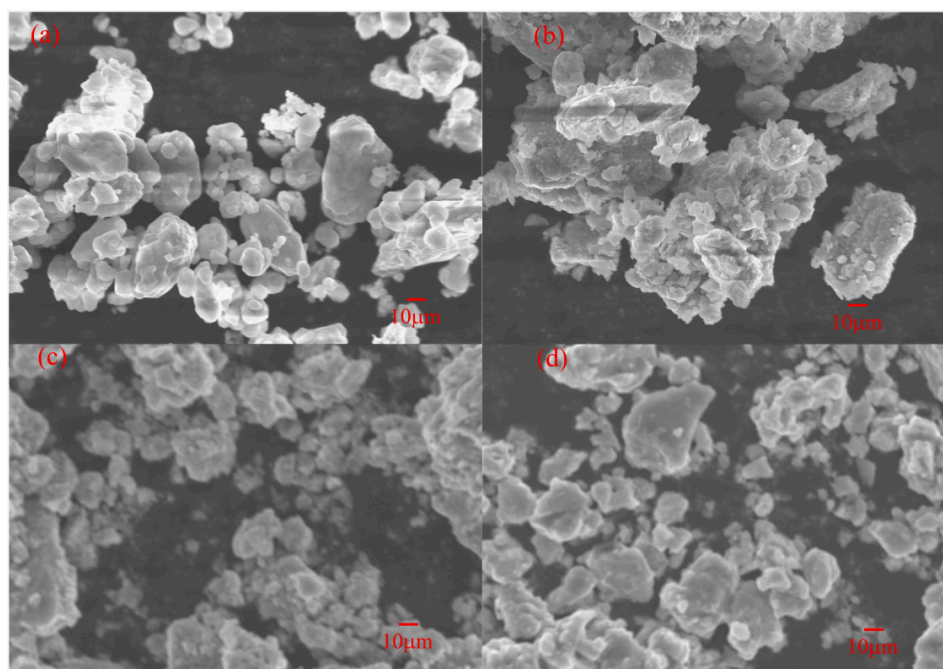


Figure 3. SEM images of the samples at different milling times. (a) 0 min, (b) 120 min, (c) 180 min, (d) 240 min. Conditions: $n_{\text{LiCoO}_2}/n_{\text{Fe}}/n_{\text{Br}} = 1.5:1.67:1$, $m_b/m_p = 100:1$, rotation speed = 600 rpm.

3.3.2. XRD Analysis

XRD patterns of milled samples before and after MC treatment are presented in Figure 4. The peaks corresponding to the crystal planes 003, 101, and 104 represent the layer structure of LiCoO_2 . It is obvious that the intensity of these peaks weakened gradually with prolonged ball milling time, indicating the destruction of the crystal structure of LiCoO_2 . Accordingly, the structure of Fe reflected by the diffraction peak of 110 crystal plane, which disappeared after milling, and the new peaks of 211 crystal plane corresponding to Fe_2O_3 were observed, showing the oxidation of $\text{Fe}(0)$ to $\text{Fe}(\text{III})$. $\text{Fe}(0)$ acted as a reducing reagent to reduce BDE 209 during the MC process. The grain size of 003 and 110 peaks decreased from about 1000 nm to 453 and 243 nm after 240 min grinding, respectively, which also indicated the decrease of LiCoO_2 and Fe (Figure S4). Furthermore, the FWHM of the two main crystal planes, 003 and 110, broadened with the increase of MC reaction time (Figure S5). Results suggest that the crystal structure of LiCoO_2 and Fe was gradually converted to an amorphous state within the process. The disorder degree (Figure S5), representing the degree of amorphousness, became higher with MC treatment time from 0 to 240 min, very consistent with the results of FWHM.

3.3.3. XPS Analysis

XPS analysis was conducted to measure the chemical state of elements in the milled samples. The XPS spectra of Br 3d, C 1s, Co 2p, O 1s, Fe 2p before and after 180 min MC treatment are presented in Figure 5a. In non-activated samples, two types of bromine, Br 3d_{5/2} and Br 3d_{3/2} with binding energies 70.8 and 71.9 eV, were attributed to covalently bonded bromine atoms in BDE 209. After 180 min grinding, two new peaks appeared at 68.8 and 69.5 eV, assigned to Br^- (Figure 5b), suggesting that the organic bromine from BDE 209 was released and transformed to Br^- [31]. The C 1s peaks at 286.4 eV and 288.8 eV, attributed to C-Br of BDE 209, disappeared after milling (Figure 5c). The peak at 284.8 eV assigned to C-C decreased significantly, and a new peak at 291.1 eV was observed. These results reveal that the organic structure of BDE 209 was decomposed

and transformed into graphitic and amorphous carbon [36]. For Co 2p (Figure 5d), the binding energies of Co 2p_{3/2} and Co 2p_{1/2} at 779.8 and 794.8 eV, respectively, belong to Co(III), consistent with Co(III) in non-activated LiCoO₂. The binding energies of Co 2p_{3/2} and Co 2p_{1/2} representing Co(II) appear at 781.3 and 796.3 eV, respectively [40], indicating that the valence state of Co was changed from Co(III) to Co(II). The XPS profile of O 1s (Figure 5e) for the sample before reaction at the peak of 529.4 eV can be fitted with the lattice oxygen in LiCoO₂ [41]. Afterwards, this peak disappeared, and the relative intensity of the peak at 532.9 eV, attributed to oxygen vacancies, significantly increased due to the MC process. This indicates that the active oxygen in LiCoO₂ can transfer electrons to the aromatic structure thus inducing the reduction of BDE 209. Fe 2p spectra are shown in Figure 5f, with binding energies of Fe 2p_{2/3} and Fe 2p_{1/2} measured at 710.8 eV and 724 eV, characteristic of Fe(III) [42]. This confirmed that Fe(0) was converted to Fe(III) and acted as the reducing agent during the treatment. From these results, it can be concluded that the reductive debromination of BDE 209 by Fe, and the subsequent oxidative abatement of debrominated products by LiCoO₂ were integrated in a concerted procedure, and as a result, leading to the elimination of BDE 209.

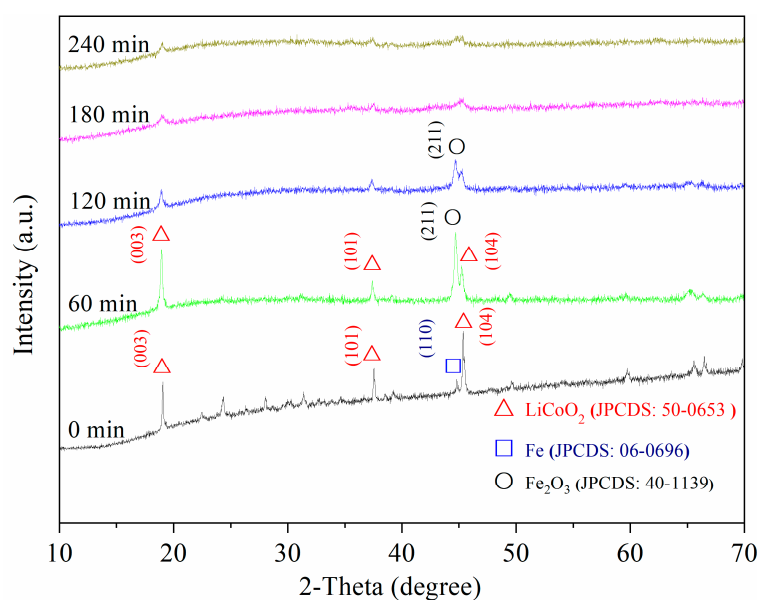


Figure 4. XRD spectra of sample at different milling times. Conditions: $n_{\text{LiCoO}_2}/n_{\text{Fe}}/n_{\text{Br}} = 1.5:1.67:1$, $m_b/m_p = 100:1$, rotation speed = 600 rpm.

3.3.4. FT-IR Analysis

The samples, both before and after MC treatment for 180 min, were prepared for FT-IR analysis. The spectra in Figure 6 offer valuable insights into the structural and functional properties of the milled samples. In non-milled samples, the peaks at 1499 and 1321 cm⁻¹ represented the chain vibrations of the aromatic ring, while the peaks at 962, 763, and 695 cm⁻¹ were attributed to the stretching vibration of the C-Br bond. Additionally, the peak at 1210 cm⁻¹ denoted the asymmetrical stretching vibration of the C-O-C bond in BDE 209 [43]. Interestingly, all the abovementioned peaks disappeared in the 180 min ball-milled sample, suggesting that BDE 209 was degraded completely, and the bromine was removed from the organic structure. These observations align with the findings from the degradation and debromination experiments.

3.3.5. Degradation Pathway of BDE 209

The degradation intermediates of BDE 209 during the MC process at different ball milling times were identified by GC-MS, as detailed in Figures S6–S8. It is evident that the peak intensity of BDE 209 weakened, and dibromodiphenyl ether, tribromodiphenyl ether, and 3,5-dibromophenol were observed after 60 min of milling. Furthermore, the

peaks of BDE 209 or low brominated aromatics disappeared after 180 min of milling, while aliphatic products such as 2-bromo-3-methyl-hexane-1,5-diol, 3-methyl-1,5-hexanediol, and 3-methyl-1-hexanol were identified (Additional mass spectral data are provided in Figures S9–S15). From all the identified intermediates, we concluded that the decomposition of BDE 209 involved a series of consecutive reactions, namely the C-Br and C-O-C bonds of BDE 209 were first broken, and low brominated aromatic products were produced during the initial period of the MC process. Subsequently, the aromatic structures underwent ring opening to generate aliphatic products; the degradation pathways of BDE 209 are proposed in Figure 7.

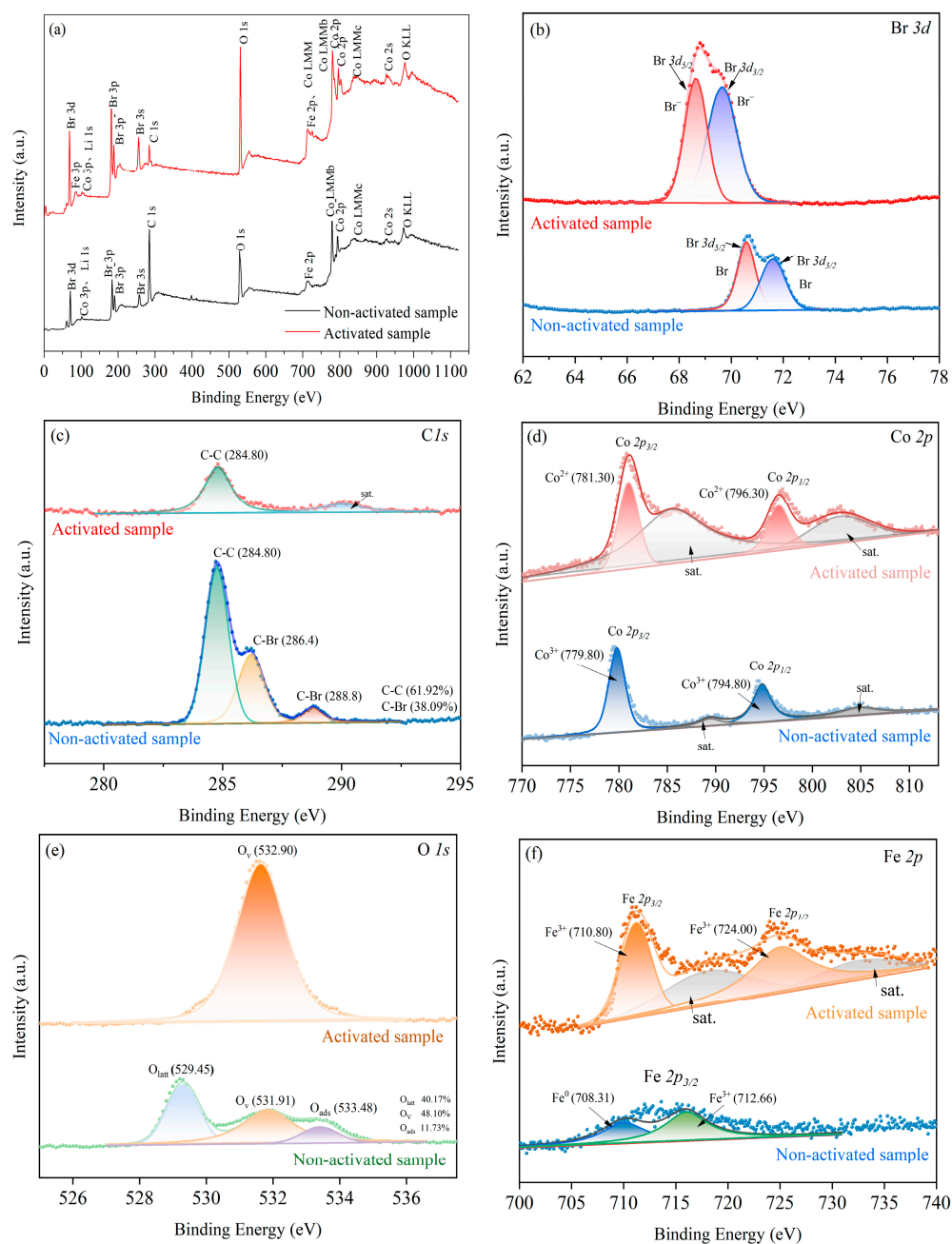


Figure 5. XPS spectra of samples before and after ball milling for 180 min. (a) Full XPS spectra analysis, (b) Br 3d XPS spectra, (c) C 1s XPS spectra, (d) Co 2p XPS spectra, (e) O 1s XPS spectra, (f) Fe 2p XPS spectra. Conditions: $n_{\text{LiCoO}_2}/n_{\text{Fe}}/n_{\text{Br}} = 1.5:1.67:1$, $m_b/m_p = 100:1$, rotation speed = 600 rpm.

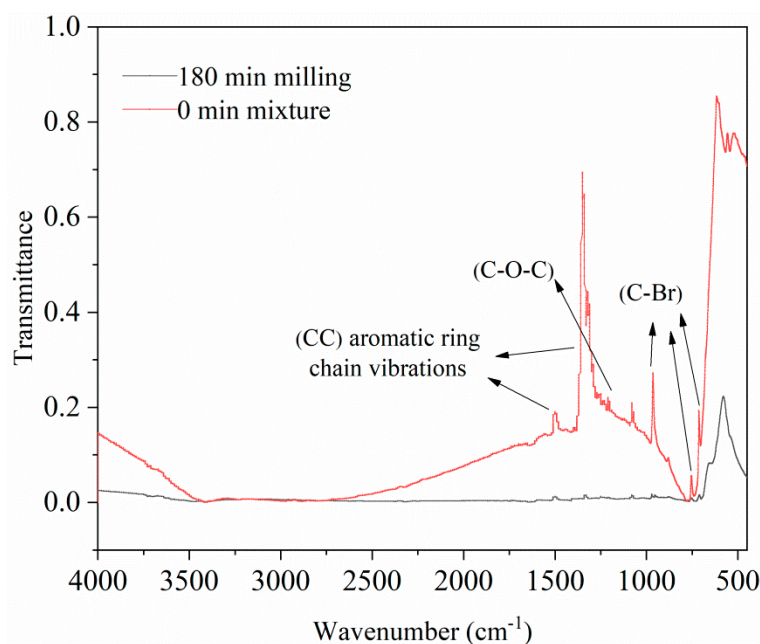


Figure 6. FT-IR spectra of samples before and after ball milling for 180 min. Conditions: $n_{\text{LiCoO}_2}/n_{\text{Fe}}/n_{\text{Br}} = 1.5:1.67:1$, $m_b/m_p = 100:1$, rotation speed = 600 rpm.

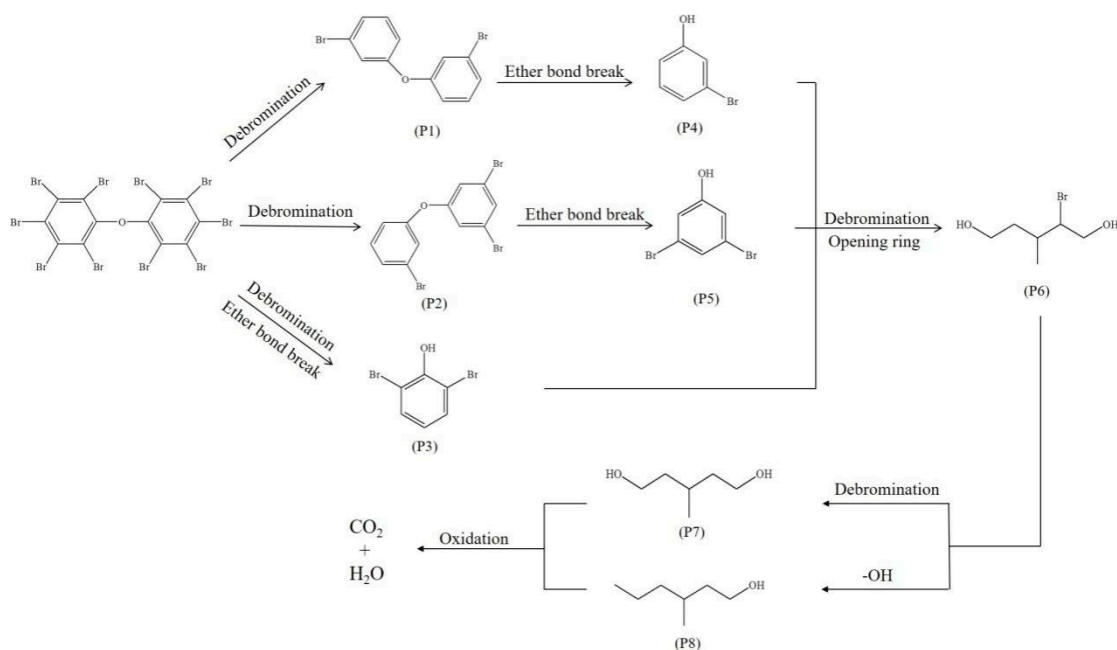


Figure 7. The possible pathways for BDE309 degradation by MC treatment with combined LiCoO_2 and Fe as co-milling reagents.

4. Conclusions

The present work first reports the degradation of BDE 209 by using MC treatment with LiCoO_2 and Fe as co-grinding agents. The favorable interaction between LiCoO_2 and Fe was found to be dependent upon the LiCoO_2 to Fe molar ratio, rotation speed, and the ball-to-powder ratio. Under optimum conditions ($n_{\text{LiCoO}_2}/n_{\text{Fe}}/n_{\text{Br}} = 1.5:1.67:1$, $m_b/m_p = 100:1$, rotation speed = 600 rpm), a 180-min ball milling in LiCoO_2 and Fe combined system resulted in a degradation efficiency of 99.8% for BDE 209. This efficiency was approximately 3.5 and 4.2 times higher than that in the Fe-only and LiCoO_2 -only system, respectively. SEM, XRD, XPS, FT-IR, and GC-MS analyses confirmed that Fe acted as the reducing agent

to initiate the debromination of BDE 209 during the MC process. The ball milling process activated the lattice oxygen of LiCoO_2 , facilitating the oxidation of the debromination products of BDE 209. Namely, during the MC process, Co(III) in LiCoO_2 was reduced to Co(II) , Fe(0) was oxidized to Fe(III) , and the organic bromine in BDE 209 was converted to dissolvable inorganic Br^- . The BDE 209 was firstly reduced to low brominated aromatic intermediates, and then decomposed to aliphatic products through ring opening triggered by the mechanical force and LiCoO_2 oxidation. These findings highlight that the MC method with co-milling reactants is a potential technology for removing BDE 209 in solid matrices. The strategy of combined utilization of LiCoO_2 and Fe as co-grinding reagents in the MC treatment proposes an alternative route for the degradation of toxic halogenated contaminants together with implementation of ball milling.

Supplementary Materials: The following supporting information can be downloaded at: <https://www.mdpi.com/article/10.3390/app132312924/s1>, Figure S1: The effect of grinding reagent molar ratio between LiCoO_2 and Fe ($n\text{LiCoO}_2/n\text{Fe}$) on the degradation of BDE209 in MC treatment. Figure S2: The effect of rotation speed on the degradation of BDE209 in MC treatment. Figure S3: The effect of ball-to-powders mass ratio (m_b/m_p) on the degradation of BDE209 in MC treatment. Figure S4: Grain size changes of different crystal planes with varying milling times. Figure S5: FWHM and disorder degree changes of different crystal planes with varying milling times. Figure S6: GC chromatogram of BDE209 before MC treatment. Figure S7: GC chromatogram of BDE209 after 60 min ball milling time. Figure S8: GC chromatogram of BDE209 after 180 min ball milling time. Figure S9: GC-MS spectrum of decabromodiphenyl ether. Figure S10: GC-MS spectrum of dibromodiphenyl ether (P1). Figure S11: GC-MS spectrum of tribromodiphenyl ether (P2). Figure S12: GC-MS spectrum of 3,5-dibromophenol (P5). Figure S13: GC-MS spectrum of 2-bromo-3-methyl-hexane-1,5-diol (P6). Figure S14: GC-MS spectrum of 3-methyl-1,5-hexanediol (P7). Figure S15: GC-MS spectrum of 3-methyl-1-hexanol (P8).

Author Contributions: Writing—original draft, X.L.; Writing—review, editing, and funding acquisition, J.G., Y.S. (Yongfu Shi), and X.L.; Validation, Q.Z. and C.F.; Visualization, Y.T. and X.Z.; Methodology and investigation, X.L. and Y.S. (Yifan Sui); Data curation: G.Y.; Supervision and funding acquisition, D.H. and Y.G. The manuscript was written with the contributions of all authors. All authors have read and agreed to the published version of the manuscript.

Funding: The present work was financially supported by the Natural Science Foundation of China (52270129, 52070127 and 52370142), the Shanghai Natural Science Foundation (20ZR1421100), and the Central-Public interest Scientific Institution Basal Research Fund (2019T13, 2019T14). Guo also thanks the financial support of the Science and Technology Development Fund of Pudong New Area (PKJ2021-C01, and PKJ2022-C07).

Institutional Review Board Statement: Not applicable.

Informed Consent Statement: Not applicable.

Data Availability Statement: The data presented in this study are available on request from the corresponding author. The data are not publicly available due to privacy.

Acknowledgments: We thank Hei Wen Kan at the City University of Hong Kong for his careful proofreading.

Conflicts of Interest: The authors declare no conflict of interest.

References

1. Wang, N.; Lai, C.; Xu, F.; Huang, D.; Zhang, M.; Zhou, X.; Xu, M.; Li, Y.; Li, L.; Liu, S.; et al. A review of polybrominated diphenyl ethers and novel brominated flame retardants in Chinese aquatic environment: Source, occurrence, distribution, and ecological risk assessment. *Sci. Total Environ.* **2023**, *904*, 166180. [[CrossRef](#)] [[PubMed](#)]
2. MJin, M.; Xu, Z.; Zhang, S.; Sun, L.; Wu, J. Pollution status, particle-size distribution and health impacts (people at different ages) of polybrominated diphenyl ethers in bedrooms. *J. Environ. Chem. Eng.* **2023**, *11*, 111289. [[CrossRef](#)]
3. Li, Y.; Yang, Y.; Tang, Y.; Dang, X.; Zhou, K.; Liu, B.; Bian, B. Optimal emission reductions pathway for polybrominated diphenyl ethers in typical household e-waste dismantling products. *Sci. Total Environ.* **2023**, *883*, 163697. [[CrossRef](#)] [[PubMed](#)]
4. Hou, R.; Lin, L.; Li, H.; Liu, S.; Xu, X.; Xu, Y.; Jin, X.; Yuan, Y.; Wang, Z. Occurrence, bioaccumulation, fate, and risk assessment of novel brominated flame retardants (NBFRs) in aquatic environments—A critical review. *Water Res.* **2021**, *198*, 117168. [[CrossRef](#)] [[PubMed](#)]

5. Gao, H.; Chen, J.; Wang, C.; Wang, P.; Wang, R.; Feng, B. Regulatory mechanisms of submerged macrophyte on bacterial community recovery in decabromodiphenyl ether contaminated sediment: Microbiological and metabolomic perspectives. *Environ. Pollut.* **2023**, *337*, 122616. [[CrossRef](#)]
6. Zhang, Y.; Xi, B.; Tan, W. Release, transformation, and risk factors of polybrominated diphenyl ethers from landfills to the surrounding environments: A review. *Environ. Int.* **2021**, *157*, 106780. [[CrossRef](#)]
7. Shi, C.; Hu, Y.; Kobayashi, T.; Zhang, N.; Kuramochi, H.; Zhang, Z.; Lei, Z.; Xu, K.-Q. Comparison of decabromodiphenyl ether degradation in long-term operated anaerobic bioreactors under thermophilic and mesophilic conditions and the pathways involved. *J. Environ. Manag.* **2021**, *294*, 113009. [[CrossRef](#)]
8. Chen, Y.; Li, J.; Tan, Q. Trends of production, consumption and environmental emissions of Decabromodiphenyl ether in mainland China. *Environ. Pollut.* **2020**, *260*, 114022. [[CrossRef](#)]
9. Hoang, A.Q.; Tran, T.M.; Tu, M.B.; Takahashi, S. Polybrominated diphenyl ethers in indoor and outdoor dust from Southeast Asia: An updated review on contamination status, human exposure, and future perspectives. *Environ. Pollut.* **2021**, *272*, 116012. [[CrossRef](#)]
10. Donaldson, D.L.; Jayaweera, D. Effective solar prosumer identification using net smart meter data. *Int. J. Elect. Power Energy Syst.* **2021**, *118*, 105823. [[CrossRef](#)]
11. Motamedi, M.; Yerushalmi, L.; Haghighat, F.; Chen, Z. A critical review of water contamination by polybrominated diphenyl ethers (PBDE) and main degradation techniques. *J. Environ. Chem. Eng.* **2022**, *10*, 108196. [[CrossRef](#)]
12. Xiong, P.; Yan, X.; Zhu, Q.; Qu, G.; Shi, J.; Liao, C.; Jiang, G. A review of environmental occurrence, fate, and toxicity of novel brominated flame retardants. *Environ. Sci. Technol.* **2019**, *53*, 13551–13569. [[CrossRef](#)] [[PubMed](#)]
13. Zhang, Z.; Wu, X.; Liu, H.; Huang, X.; Chen, Q.; Guo, X.; Zhang, J. A systematic review of microplastics in the environment: Sampling, separation, characterization and coexistence mechanisms with pollutants. *Sci. Total Environ.* **2023**, *859*, 160151. [[CrossRef](#)] [[PubMed](#)]
14. Cheng, L.; Yang, J.; Rao, Q.; Liu, Z.; Song, W.; Guan, S.; Zhao, Z.; Song, W. Toxic effects of Decabromodiphenyl ether (BDE-209) on thyroid of broiler chicks by transcriptome profile analysis. *Ecotoxicol. Environ. Saf.* **2021**, *219*, 112305. [[CrossRef](#)] [[PubMed](#)]
15. Qian, B.; Wang, C.; Zhao, C.; Jiang, R.; Song, J. Effects of maternal exposure to BDE 209 on neuronal development and transcription of iodothyronine deiodinase in offspring mice. *Toxicol. Mech. Methods* **2019**, *29*, 569–579. [[CrossRef](#)] [[PubMed](#)]
16. Cheng, F.; He, J.; Li, C.; Lu, Y.; Zhang, Y.-N.; Qu, J. Photo-induced degradation and toxicity change of decabromobiphenyl ethers (BDE-209) in water: Effects of dissolved organic matter and halide ions. *J. Hazard. Mater.* **2021**, *416*, 125842. [[CrossRef](#)]
17. Zhang, Z.; Wu, X.; Zhang, J.; Huang, X. Distribution and migration characteristics of microplastics in farmland soils, surface water and sediments in Caohai Lake, southwestern plateau of China. *J. Clean. Prod.* **2022**, *366*, 132912. [[CrossRef](#)]
18. Lei, M.; Wang, N.; Zhu, L.; Zhou, Q.; Nie, G.; Tang, H. Photocatalytic reductive degradation of polybrominated diphenyl ethers on CuO/TiO₂ nanocomposites: A mechanism based on the switching of photocatalytic reduction potential being controlled by the valence state of copper. *Appl. Catal. B Environ.* **2016**, *182*, 414–423. [[CrossRef](#)]
19. Nguyen, V.-H.; Smith, S.M.; Wantala, K.; Kajitvichyanukul, P. Photocatalytic remediation of persistent organic pollutants (POPs): A review. *Arabian J. Chem.* **2020**, *13*, 8309–8337. [[CrossRef](#)]
20. Dong, Y.; Li, Y.; Zhao, C.; Feng, Y.; Chen, S.; Dong, Y. Mechanism of the rapid mechanochemical degradation of hexachlorobenzene with silicon carbide as an additive. *J. Hazard. Mater.* **2019**, *379*, 120653. [[CrossRef](#)]
21. Wang, N.; Lv, H.; Zhou, Y.; Zhu, L.; Hu, Y.; Majima, T.; Tang, H. Complete Defluorination and Mineralization of Perfluorooctanoic Acid by a Mechanochemical Method Using Alumina and Persulfate. *Environ. Sci. Technol.* **2019**, *53*, 8302–8313. [[CrossRef](#)] [[PubMed](#)]
22. Liang, Y.; Min, X.; Chai, L.; Wang, M.; Liyang, W.; Pan, Q.; Okido, M. Stabilization of arsenic sludge with mechanochemically modified zero valent iron. *Chemosphere* **2017**, *168*, 1142–1151. [[CrossRef](#)] [[PubMed](#)]
23. Deng, S.; Kang, S.; Feng, N.; Zhu, J.; Yu, B.; Xie, X.; Chen, J. Mechanochemical mechanism of rapid dechlorination of hexachlorobenzene. *J. Hazard. Mater.* **2017**, *333*, 116–127. [[CrossRef](#)] [[PubMed](#)]
24. Li, X.; Chen, M.; Li, G.; Wang, P. Constructing MnO₂ alpha/amorphous heterophase junction by mechanochemically induced phase transformation for formaldehyde oxidation. *Appl. Surf. Sci.* **2022**, *589*, 152855. [[CrossRef](#)]
25. Huang, A.; Zhang, Z.; Wang, N.; Zhu, L.; Zou, J. Green mechanochemical oxidative decomposition of powdery decabromodiphenyl ether with persulfate. *J. Hazard. Mater.* **2016**, *302*, 158–165. [[CrossRef](#)]
26. Zhang, W.; Huang, J.; Xu, F.; Deng, S.; Zhu, W.; Yu, G. Mechanochemical destruction of pentachloronitrobenzene with reactive iron powder. *J. Hazard. Mater.* **2011**, *198*, 275–281. [[CrossRef](#)]
27. Nasser, A.; Mingelgrin, U. Birnessite-induced mechanochemical degradation of 2,4-dichlorophenol. *Chemosphere* **2014**, *107*, 175–179. [[CrossRef](#)]
28. Deng, S.; Bao, Y.; Cagnetta, G.; Huang, J.; Yu, G. Mechanochemical degradation of perfluorohexane sulfonate: Synergistic effect of ferrate(VI) and zero-valent iron. *Environ. Pollut.* **2020**, *264*, 114789. [[CrossRef](#)]
29. Zhang, W.; Wang, H.; Jun, H.; Yu, M.; Wang, F.; Zhou, L.; Yu, G. Acceleration and mechanistic studies of the mechanochemical dechlorination of HCB with iron powder and quartz sand. *Chem. Eng. J.* **2014**, *239*, 185–191. [[CrossRef](#)]
30. Li, Q.; Yang, S.; Wu, S.; Fan, D. Mechanochemically synthesized Al-Fe (oxide) composite with superior reductive performance: Solid-state kinetic processes during ball milling. *Chemosphere* **2022**, *298*, 134280. [[CrossRef](#)]

31. Zhang, Z.; Wang, N.; Zhu, L.; Lv, H.; Dong, X.; Chai, H.; Tang, H. Synergistic effect between Fe and Bi₂O₃ on enhanced mechanochemical treatment of decabromodiphenyl ether. *J. Environ. Chem. Eng.* **2017**, *5*, 915–923. [[CrossRef](#)]
32. Saeki, S.; Lee, J.; Zhang, Q.; Saito, F. Co-grinding LiCoO₂ with PVC and water leaching of metal chlorides formed in ground product. *Int. J. Miner. Process.* **2004**, *74*, S373–S378. [[CrossRef](#)]
33. Guan, J.; Li, Y.; Guo, Y.; Su, R.; Gao, G.; Song, H.; Yuan, H.; Liang, B.; Guo, Z. Mechanochemical process enhanced cobalt and lithium recycling from wasted lithium-ion batteries. *ACS Sustain. Chem. Eng.* **2016**, *5*, 1026–1032. [[CrossRef](#)]
34. Chen, Z.; Lu, S.; Mao, Q.; Buekens, A.; Wang, Y.; Yan, J. Energy transfer and kinetics in mechanochemistry. *Environ. Sci. Pollut. Res.* **2017**, *24*, 24562–24571. [[CrossRef](#)] [[PubMed](#)]
35. Guo, Y.; Li, Y.; Lou, X.; Guan, J.; Li, Y.; Mai, X.; Liu, H.; Zhao, C.X.; Wang, N.; Yan, C.; et al. Improved extraction of cobalt and lithium by reductive acid from spent lithium-ion batteries via mechanical activation process. *J. Mater. Sci.* **2018**, *53*, 13790–13800. [[CrossRef](#)]
36. Chai, H.; Zhang, Z.; Zhou, Y.; Zhu, L.; Lv, H.; Wang, N. Roles of intrinsic Mn³⁺ sites and lattice oxygen in mechanochemical debromination and mineralization of decabromodiphenyl ether with manganese dioxide. *Chemosphere* **2018**, *207*, 41–49. [[CrossRef](#)] [[PubMed](#)]
37. Wang, R.; Zhu, Z.; Tan, S.; Guo, J.; Xu, Z. Mechanochemical degradation of brominated flame retardants in waste printed circuit boards by Ball Milling. *J. Hazard. Mater.* **2020**, *385*, 121509. [[CrossRef](#)] [[PubMed](#)]
38. Mio, H.; Saeki, S.; Kano, J.; Saito, F. Estimation of Mechanochemical Dechlorination Rate of Poly(vinyl chloride). *Environ. Sci. Technol.* **2002**, *36*, 1344–1348. [[CrossRef](#)]
39. Yi, Y.; Kou, F.; Tsang, P.E.; Fang, Z. Highly efficient remediation of decabromodiphenyl ether-contaminated soil using mechanochemistry in the presence of additive and its mechanism. *J. Environ. Manag.* **2021**, *299*, 113595. [[CrossRef](#)]
40. Zhao, Y.; Yuan, X.; Jiang, L.; Li, X.; Zhang, J.; Wang, H. Reutilization of cathode material from spent batteries as a heterogeneous catalyst to remove antibiotics in wastewater via peroxydisulfate activation. *Chem. Eng. J.* **2020**, *400*, 125903. [[CrossRef](#)]
41. Meng, Q.; Zhang, Y.; Dong, P. Use of electrochemical cathode-reduction method for leaching of cobalt from spent lithium-ion batteries. *J. Clean. Prod.* **2018**, *180*, 64–70. [[CrossRef](#)]
42. Nie, M.; Li, Y.; Dong, Y.; Song, Z.; Zhao, C.; Chen, S. Mechanochemical degradation of hexachlorobenzene with a combined additive of SiC and Fe. *Chem. Eng. Res. Des.* **2022**, *177*, 167–173. [[CrossRef](#)]
43. Li, H.; Zhu, F.; He, S. The degradation of decabromodiphenyl ether in the e-waste site by biochar supported nanoscale zero-valent iron/persulfate. *Ecotoxicol. Environ. Saf.* **2019**, *183*, 109540. [[CrossRef](#)] [[PubMed](#)]

Disclaimer/Publisher’s Note: The statements, opinions and data contained in all publications are solely those of the individual author(s) and contributor(s) and not of MDPI and/or the editor(s). MDPI and/or the editor(s) disclaim responsibility for any injury to people or property resulting from any ideas, methods, instructions or products referred to in the content.